FERMILAB-CONF-19-493-AD-APC

Schemes of Laser Muon Acceleration: ultra-short, micron-scale beams

Aakash A. Sahai

College of Engineering and Applied Science
University of Colorado, Denver, CO 80204
aakash.sahai@gmail.com

Toshiki Tajima

Department of Physics & Astronomy and Applied Physics
University of California, Irvine, CA 92697

Vladimir Shiltsev

Accelerator Division, Fermi National Accelerator Laboratory
Batavia, IL 60510

Experimentally accessible schemes of laser muon ($\mu^{\pm}$) acceleration are introduced and modeled using a novel technique of controlled laser-driven post-processing of cascade showers (or pair plasmas). The proposed schemes use propagating structures in plasma, driven as wakefields of femtosecond-scale high-intensity laser, to capture particles of divergent cascade shower of: (a) hadronic type from proton-nucleon or photo-production reactions or, (b) electromagnetic type. Apart from the direct trapping and acceleration of particles of a raw shower in laser-driven plasma, a conditioning stage is proposed to selectively focus only one of the charge states. Not only is the high gradient that is sustained by laser-driven plasma structures well suited for rapid acceleration to extend the lifetime of short-lived muons but their inherent spatiotemporal scales also make possible production of unprecedented ultrashort, micron-scale muon beams. Compact laser muon acceleration schemes hold the promise to open up new avenues for applications.

Keywords: Laser-Plasma Muon Acceleration; Muon-Antimuon Pair-plasma.

1. Laser Wakefield Particle Acceleration in Gaseous Plasmas

Laser-plasma electron accelerators[1] enabled by Chirped-Pulse Amplified (CPA) lasers[2] are now capable of producing several GeV[3] electron (e^-) beams in centimeter-scale gas plasmas. These widely prototyped accelerators have demonstrated propagating acceleration structures, driven as wakefields of a CPA laser pulse, that sustain average gradients of several tens of GVm^{-1} and acceleration of a few percent energy spread e^- beams in centimeter-scale gas plasmas.

Apart from this, a two-stage laser e^- accelerator[4] and a laser positron (e^+) accelerator[5] are also under active investigation[6]. These advances in acceleration techniques coupled with the rapid ongoing development of CPA lasers open up the possibility of an affordable high-energy physics (HEP) e^+-e^- collider[7] at the energy-frontier. Orders of magnitude increase in acceleration gradients is expected to enable significant reduction in the size and cost of accelerator machines that underlie a collider. Apart from high-energy physics, these compact accelerators are

This manuscript has been authored by Fermi Research Alliance, LLC under Contract No. DE-AC02-07CH11359 with the U.S. Department of Energy, Office of Science, Office of High Energy Physics.

also expected to have a wide variety of applications in medical[8], light-source and imaging technologies[9].

However, laser acceleration of exotic particles remains largely unexplored. Laser acceleration of positrons in gaseous plasmas has been introduced using an innovative model of controlled interaction of positron-electron pair plasmas or particle showers with laser driven plasmas[5]. There have been recent efforts towards experimental prototyping of laser positron accelerator[6].

In this work we introduce mechanisms of laser acceleration of muon ($\mu^{\pm}$)[10], an exotic fundamental particle which as a second generation lepton. The mechanism introduced here follows the same methodology as the laser positron accelerator[5] and is well within the reach of the experimental capabilities of existing laser-plasma and RF acceleration test facilities. We propose and analyze the short-term experimental viability of various muon production schemes and demonstrate the processing and acceleration of the generated muons using laser-driven plasmas.

In section 2, scientific and technological applications of muons are reviewed and the potential of a compact muon source towards novel applications is discussed. Existing and well-studied techniques of muon production using conventional methods such as beams from traditional RF accelerators as well as techniques that utilize novel physics of uncommon interaction processes are reviewed in section 3. The parameter regime for laser muon acceleration in gaseous plasmas is explored in section 4 and the muon-antimuon source parameters desired for matching to laser-driven plasma acceleration structures are identified.

An evaluation of three distinct mechanisms for micron-scale muon and antimuon production, whose source properties are matched to the laser acceleration parameters as discussed section 4 and that are suitable for feeding a laser muon accelerator, are presented in sections 5. The experimental viability of these schemes of muon production for conversion efficiency and matching to a laser-driven post-processing stage is also analyzed. Preliminary Particle-In-Cell simulations are presented in section 6, to demonstrate the trapping and acceleration of muons produced as part of cascade showers using photo-production method. In section 7, a mechanism for segregation of oppositely charged species of muons by selective focusing is proposed and examined using a plasma lens.

The paper concludes by summarizing various sections and a plan for future work. An important part of the future work and application of ultrashort, micron-scale muon beam is for their injection into crystal wakefield accelerators such as attosecond x-ray pulse or submicron charged particle beam driven[11–13] or submicron particle beam driven solid-state tube accelerators[14,15]. The main advantage of using muons in solid-state particle accelerators is that being second generation leptons with mass around 200 times that of first generation leptons, electrons and positrons, their synchrotron radiation losses that are $\propto (m_e/m_\mu)^4$ in high focusing fields of a plasma wave are vastly reduced. Moreover, the radiative losses (including bremsstrahlung and pair production) of muons also favorably scale as $\propto (m_e/m_\mu)^2$.

Also, muons can possibly be accelerated to very high energies in a single stage continuous focusing system of crystal or CNT-based linacs[16].

2. Significance and Applications of Muons ($\mu^{\pm}$)

A compact muon source is attractive due to the distinct properties that are inherently embodied in muons. These unique properties of muons in comparison with particles that have been conventionally accessible for various applications like electrons ($e^{\pm}$), photons (γ) or protons (p, $\bar{p}$), have not only been key to enable a wide range of technologies[17] but have also played a pivotal role in exploration of an alternative energy-frontier collider design. Being a heavier lepton, the point-like characteristic of muon despite its higher mass, $m_{\mu} \simeq 207 m_e$ provides precision of collision point energy over p-p or p-$\bar{p}$ collisions[18]. Moreover being heavier than $e^{\pm}$, muons have lower synchrotron radiation ($\propto m_{\mu}^{-4}$, over $e^{\pm}$) and radiative losses ($\propto m_{\mu}^{-2}$, over $e^{\pm}$) even at higher energies (E_{μ}) which enables deeper penetration depth in materials and greater stability of high E_{μ} storage-rings. The weak force mediated $\mu^{\pm}$ decay ($\tau_{\mu} \simeq 2.2\mu\mathrm{s}\ \mathrm{E}_{\mu}/\mathrm{m}_{\mu}$)[19] has permitted neutrino flavor oscillation studies ($\nu/\bar{\nu}_{\mathrm{e},\mu}$) through high-intensity ($\mathrm{N}_{\nu} \propto \mathrm{E}_{\mu}^{>2}$) ν-production[20]. Muon sources however currently demand many tens of meters of proton accelerators[21] under $100\mathrm{MVm}^{-1}$ gradient limit[22].

Due to lack of affordable technologies for controlled muon sources available thus far, raw cosmic $\mu^{\pm}$ flux from extensive air showers ($1\mathrm{cm}^{-2}\mathrm{min}^{-1} \gtrsim 1\mathrm{GeV}$ with $\cos^2\theta$ fall-off from vertical) has been used in an expanding range of applications of muography[17] in nuclear threat detection[23], archaeology[24], geosciences[25] that require long stopping range ($\mathrm{E}_{\mu} \gtrsim 1\mathrm{GeV}$). Slow $\mu^{\pm}$ with short stopping range, from lab-based sources are also widely used in material[26], molecular[27] and medical sciences[28] etc. through $\mu^{\pm}$ spin relaxation (μSR) spectroscopy[29]. Muons are also attractive for research in areas like true-muonium[30] (μ^{+}-μ^{-}) atomic physics and μ^{-}-catalyzed fusion[31] etc.

Development of compact and tunable muon sources with controllable E_{μ} spectrum, ultra-short bunch lengths and micron-scale transverse properties, as studied here, is therefore attractive not only for technological but also for HEP applications[11–15] which additionally demand high average flux and ultra-low emittance.

3. Conventional $\mu^{\pm}$ Sources: Hadronic shower and Direct production

Conventionally, production of muons in a laboratory environment has been realized using several distinct processes.

Hadronic showers[32], produced through proton-nucleon reactions when hundreds of MeV proton beams[33,34] strike targets, predominantly contain $\pi^{\pm}$-mesons (pions and fractionally other mesons), with large energy and angular spread, that undergo spin-polarized decay to $\mu^{\pm}$[32].

Hadronic $\pi^{\pm}$-$\mu^{\pm}$ showers also produced through photo-meson reaction[37] have been modeled using $\gtrsim$ 140MeV electron beam undergoing bremsstrahlung in a target to produce MeV-scale $\pi^{\pm}$ that decay to $\mu^{\pm}$. At electron beam energies near $\pi^{\pm}$ mass, photo-pion production process dominates whereas contributions of other simultaneous processes towards $\pi^{\pm}$-meson production such as Bethe-Heitler (BH) $\mu^{\pm}$ pair production mediated by a nuclei and $\pi^{\pm}$ electro-production (trident-like) process mediated by virtual photons during inelastic scattering of electrons off of a nuclei, is relatively small.

Efficient $\mu^{\pm}$ production from hadronic showers demands methods for confinement of the divergent $\pi^{\pm}$-$\mu^{\pm}$ flux[35,36]. A high proton to $\mu^{\pm}$ yield requires methods[21,35] to capture and rapidly accelerate $\mu^{\pm}$ from hadronic showers to many times the rest-mass energy of muons over $\lesssim c\tau_{\mu}$ [18] as well as to simultaneously cool the $\mu^{\pm}$ phase-space obtained from the divergent $\pi^{\pm}$-$\mu^{\pm}$ flux. Moreover, $\pi^{\pm}$-decay lifetime demands many meters long confinement channel ($c\tau_{\pi} \approx 8E_{\pi}/m_{\pi}\ m$)[38].

Direct $\mu^{\pm}$ production processes have also been studied. BH muon pair production using an electron beam of much higher-energy than $\pi^{\pm}$-$\mu^{\pm}$ rest mass undergoing bremsstrahlung is well established[39]. Direct $\mu^{\pm}$ production using e^{-}-photon scattering[40] requires head-on collision between GeV-scale e^{-} beam and tens of MeV photons[41]. But, scaling up the yield and energy spectrum of MeV-scale photon itself relies on a high-degree of precision to make possible Compton scattering interaction. Breit-Wheeler (BW)[42] $\mu^{\pm}$ pair production (time-reversal symmetry of $\mu^{\pm}$ annihilation), as opposed to BH pair production, requires $\gtrsim$ 212MeV center-of-mass photon-photon collision which significantly increases the complexity of simultaneous control over two hundreds of MeV photon sources (in contrast with BH process which requires one photon and a heavy nuclei).

Beam mediated direct $\mu^{\pm}$ production from photons interacting with a relativistic nuclei[43] not only requires hundred MeV-scale photons possibly being obtained using bremsstrahlung but also a highly relativistic ion beam. Nonlinear BW process (multi-photon) is more accessible using CPA lasers but suffers from ultra-low yield. Direct $\mu^{\pm}$ production using e^{+} and e^{-} annihilation in a stationary target[45] which requires $\gtrsim$ 43GeV e^{+} beam and Relativistic heavy ion collisions[46] both depend on kilometer-scale machines. Resonant annihilation during ring stored e^{+} and e^{-} beams to directly produce $\mu^{\pm}$ pairs also requires hundreds of meters of rf accelerators[47].

With the advent of advanced acceleration methods[1] laser-driven electron accelerators have been proposed for hadronic shower production using laser-plasma accelerated (LPA) multi-GeV e^{-} interacting with a target has been modeled[48]. Compact and tunable $\mu^{\pm}$ sources and corresponding laser muon acceleration schemes however still remain vastly unstudied and thus yet unrealized.

4. Laser Muon ($\mu^{\pm}$) Acceleration: Rapid Acceleration, Ultrashort Bunches & Micron Spot-size

In this paper, compact and tunable schemes of laser muon acceleration are proposed and studied. These schemes of laser muon acceleration are based upon the interaction of controlled laser-driven plasma sustaining traveling plasma density structures with matched laser produced cascade showers which when under external confinement are also labelled as pair or exotic matter plasmas. The process of matching of cascade shower characteristics such as its energy spectra and transverse phase parameters is explored here.

4.1. *Properties of laser wakefield acceleration structures in plasmas*

The acceleration and focusing gradients ($E_{\rm plasma}$) inherently sustained in laser-driven plasmas[1]:

$$E_{\rm plasma} \simeq \sqrt{n_0(10^{20}cm^{-3})}\ TVm^{-1} \tag{1}$$

where n_0 is the plasma electron density, are especially well suited for trapping and acceleration of short lifetime (τ_π, τ_μ) particles. Trapping short lifetime heavier particles ($\pi^{\pm}$,$\mu^{\pm}$) that are predominantly produced from the source at a small fraction of the speed of light required that the velocity of the laser-driven structures is small enough to allow significant interaction time. The plasma density also plays a critical role as the group velocity of a laser ($\beta_{\rm g}^{\rm laser}$) and thus of the co-propagating acceleration structure in the plasma (β_{acc}) is:

$$\beta_{\rm g}^{\rm laser} \simeq \beta_{\rm acc} \simeq \sqrt{1 - \frac{1}{10\pi}\ n_0(10^{20}cm^{-3})\ \lambda_0^2(\mu m)\ r_e(fm)} \tag{2}$$

where, λ_0 is the laser wavelength and r_e is the classical electron radius, 2.818 fm.

Rapid acceleration within the lifetime of unstable particles to many times their rest-mass energy, using high-gradient laser-driven acceleration structures, extends their lifetime proportional to the Lorentz factor acquired through acceleration. This rapid extension of lifetime enabled by high-gradient laser acceleration thus increases the efficacy of unstable particles for applications.

While the high focussing fields are quite effective for initial trapping, muons being a heavier lepton undergo smaller transverse oscillations driven radiation losses under off-axis displacement relative to electrons interacting with equivalent fields.

Moreover, the natural dimension of laser acceleration structures in plasma is of the order of plasma wavelength ($\lambda_{\rm plasma}$),

$$\lambda_{\rm plasma} \simeq \frac{3.3}{\sqrt{n_0(10^{20}cm^{-3})}}\ \mu{\rm m}\ \simeq {\rm L_{beam}, r_{beam}} \tag{3}$$

which makes possible for the spot-size of the accelerated particle beams ($r_{\rm beam}$) to be micron scale in plasma. Similarly, the bunch-lengths ($L_{\rm beam}$) when using laser accelerators is also of the order of the plasma wavelength which has a range of a

few to tens of microns. Thus, the muon beam when accelerated within a plasma acceleration structure is not only micron-scale transversely but also has an ultra-short bunch-length. This inherently micron-scale dimensionality of the acceleration structures makes possible unprecedented energy density of exotic particle beams when accelerated using laser accelerator schemes, as proposed here, if a sufficient number of exotic particles are effectively produced and trapped.

For a Ti:Sapphire CPA laser with characteristic center wavelength, $\lambda_0 = 0.8\mu m$, laser group velocity (β_g^{laser}, eq.2) and plasma wavelength (λ_{plasma}, eq.3) with plasma density is shown in Fig.1.

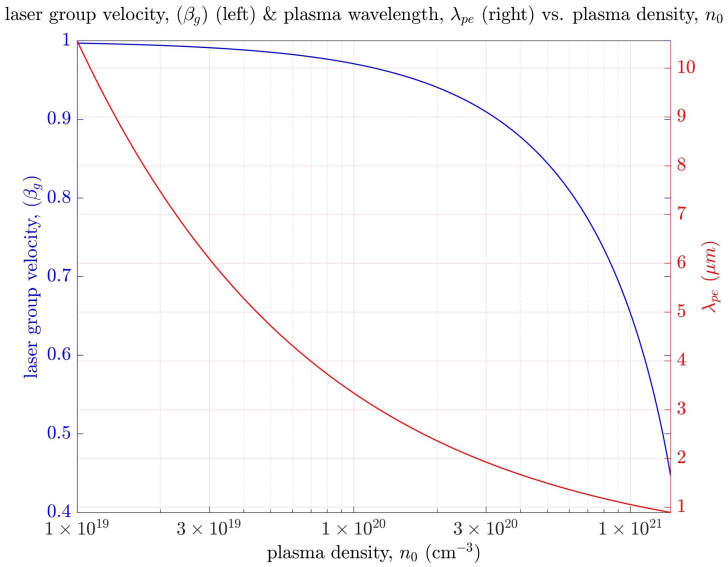

Fig. 1. Laser group velocity (β_g^{laser}, eq.2) and plasma wavelength (λ_{plasma}, eq.3) with plasma density for a Ti:Sapphire (active medium) CPA laser with central wavelength, $\lambda_0 = 0.8\mu m$.

4.2. *Matching of cascade showers with laser-driven plasmas*

As evident from the micron-scale sizes of acceleration structure in laser-driven plasma it is however important that the exotic particle source that couples the particles into the acceleration structure is precisely controllable. The source should have the ability to constrain the produced exotic particles within a small transverse spot-size in addition to producing an energy spectrum which optimizes the capture efficiency through longitudinal interaction dynamics.

Therefore, it is quite critical to understand various limits under which mechanisms that produce cascade shower can deliver a micron-scale spot-size to match with the transverse size of the laser acceleration structures or at least be of the same order of size. For further enhancement of the efficiency of capture from these exotic particle sources it is essential to understand and control its energy spectra and transverse phase-space properties by varying the beam and target properties. Through detailed characterization of shower properties over the drive beam and

target property parameter-space the laser post-processing stage can be optimized to match with the characteristics of the shower.

The exotic particles produced from a controlled source are post-processed using a laser-driven plasma acceleration structure. The laser-driven plasma acceleration structure may be a plasma wave or a slowly propagating charge separation structure. By varying the laser-plasma properties of the post-processing stage the proposed schemes seek to enable a match with the pair plasma properties.

In this paper, schemes of laser muon acceleration are proposed, as listed below, and examined:

(1) Laser-driven post-processing of electron and/or positron beam driven hadronic shower to trap and accelerate muon as well as pion pairs.

(2) Laser-driven post-processing of proton beam driven hadronic showers to trap and accelerate muon as well as pion pairs.

(3) Laser-driven positron-electron storage ring for tunable muon pair production through positron-electron annihilation.

Apart from the direct interaction between cascade showers and laser-driven plasma wave, it is also possible to segregate a species of one charge state before the interactions. To enable this indirect interaction with a conditioned cascade shower, a plasma lens[52] is proposed to be inserted between the production and post-processing stage. In the conditioning state, the discharge current direction (sign of the external voltage) decides the sign of the particle species that will get focused by the plasma lens.

5. Matched Muon ($\mu^{\pm}$) Production for Laser-Plasma Muon Acceleration

In this section, we present the underlying mechanisms and corresponding analytical evaluation of muon-antimuon production schemes that produce muon phase-space that are likely to be matched with the laser muon accelerator properties outlined in section 4.

5.1. *Scheme I: Laser-driven plasma based post-processing of photo-produced hadronic shower ($e^{\pm}$-beam driven)*

Electron and positron beams undergo bremsstrahlung radiation loss when propagating in materials as they experience change in velocity due to the electromagnetic force of the material nuclei in their propagation path. The energy of the radiation emitted depends inversely on square of the particle mass undergoing bremsstrahlung. The rate of energy loss of the particle is known to be directly proportional to the particle energy ($dE/dx = E/X_0$, where, E is the nominal energy of an arbitrary particle undergoing bremsstrahlung radiation, x is the coordinate along penetration in the material and X_0 is the radiation length of the material.

From its definition, X_0 is the penetration depth at which the particle energy reduces to $1/e$ of its initial value). The photon energy spectrum follows the Bethe-Heitler (BH) function, $d\sigma_\gamma/d\varepsilon_\gamma = \frac{4}{3}\frac{1}{X_0}\ F(\varepsilon_\gamma, E_\square)\ \varepsilon_\gamma^{-1}$, where $F(\varepsilon_\gamma) \simeq 1 - \frac{\varepsilon_\gamma}{E_\square} + \frac{3}{4}\left(\frac{\varepsilon_\gamma}{E_\square}\right)^2$. It is to be noted that as in the discussion in Tsai (1974)[39], BH formalism does not include several effects attributed to the nuclei in the material such as screening of nuclear field by atomic electrons and the shape of the nuclei etc.

Bremsstrahlung radiation from an electron or positron beam with energies much higher than the rest-mass energy of muons and pions ($E_{e^\pm} \gg 140$MeV) trigger photo-production reactions in the presence of the nuclei in materials:

(R.1) photo-meson reaction:
$\gamma + p \rightarrow \pi^+ + n$
$\gamma + n \rightarrow \pi^- + p$
$\gamma + Z_1 \rightarrow \pi^\square + Z_2$, and

(R.2) Bethe-Heitler muon pair-production reaction:
$\gamma + Z \rightarrow \mu^+\mu^- + Z$

These reactions result in the production of $\mu^\pm$(-$\pi^\pm$) flux in addition to the $e^\pm$ electromagnetic shower (primarily through the BH positron-electron pair-production process). The photo-meson reaction in (R.1), that produces $\pi^\pm$ flux through bremsstrahlung photon interaction with the nuclei has a differential cross section which is at least one order of magnitude higher than that of the BH muon pair-production. But, for centimeter-scale thick targets it is expected that the $\pi^\pm$ flux component gets suppressed and de-collimated due to absorption and scattering off of the nuclei after pions are produced. On the contrary, thinner targets while increasing the $\pi^\pm$ flux result in the suppression of the $\mu^\pm$ flux.

These photo-production reactions, (R.1) and (R.2), dominate the production of hadronic $\mu^\pm$ showers. The inelastic electron scattering reaction, $e + Z \rightarrow e' + Z + \pi^\square$ has a differential cross-section which is less than about 1% of the cross section of above reactions when the electron energy is much higher than the threshold energy of $\sim$ 140 MeV. This considerably smaller differential cross-section for the inelastic scattering process in the eZ process is due to the extra electromagnetic vertex associated with a virtual photon, $d\sigma_{eZ} \propto \alpha^4 Z^2$ as compared to $d\sigma_{\gamma Z} \propto \alpha^3 Z^2$.

The cross-section of BH muon pair-production has been estimated over a wide range of parameters. In the case where the electron or positron beam that is used is ultra-relativistic ($\gamma_{e^\pm} \gg 1$) such that the typical bremsstrahlung photon energy, ε_γ is much higher than muon pair rest-mass 2 $m_\mu c^2$, then the integrated cross-section of the photo-production reaction, $\gamma + Z \rightarrow \mu^+\mu^- + Z$ can be simplified[48].

$$
\begin{aligned}
\varepsilon_\gamma &\gg 2m_\mu c^2 \\
\varepsilon_\gamma \sim E_{e^\pm} &\gtrsim 3 \text{ GeV (for validity of below BH cross-section)} \\
\sigma_{\gamma Z_1 \to \mu^+\mu^- Z_2} &\simeq \frac{28}{9}\, Z^2\, \alpha\, {r_0^\mu}^2 \left(\ln\frac{2\varepsilon_\gamma}{m_\mu c^2} - \frac{109}{42}\right) \\
\sigma_{\gamma Z_1 \to \mu^+\mu^- Z_2} &\simeq 10^{-31} m^{-2} = 0.5 \text{ milli-barn } (\varepsilon_\gamma \sim 200\text{MeV}, Z \sim 79)
\end{aligned}
\tag{4}
$$

where,

r_0^μ the classical muon radius ($r_0^\mu = 1.36 \times 10^{-17}$m), $r_0^\mu = r_0^e \times m_e/m_\mu$ where $r_0^e = r_0 = e^2 m_e^{-1} c^{-2}$(in cgs) is the classical electron radius ($r_0^e = 2.82 \times 10^{-15}$m)

Z is the atomic number of the material nuclei

α is the fine structure constant $= v_B/c = e^2\hbar^{-1}c^{-1} = r_0/\lambda\!\!\!^{-}_c = e^2(m_e c^2)^{-1}(\hbar m_e^{-1} c^{-1})$(cgs), where v_B is the velocity of the first orbit of a Bohr atom, $\lambda\!\!\!^{-}_c$ is the reduced Compton wavelength

ε_γ is energy of bremsstrahlung photon

The inefficiency of the muon pair BH photo-production process using an electron beam from a conventional rf accelerator relative to the positron-electron BH pair production process is well known[49] and is due to the smaller cross-section of the muon pair-production process by a factor of $(m_e/m_\mu)^2 \sim 1/(207)^2$.

The BH muon pair-production event rate $\mathcal{R}_{\gamma Z_1 \to \mu^+\mu^- Z_2} \equiv dN_{\mu^\pm} dt^{-1}$ can be estimated using $\mathcal{R}_{\gamma Z_1 \to \mu^+\mu^- Z_2} \equiv \frac{dN_{\mu^\pm}}{dt} = \mathcal{L} \times \sigma_{\gamma Z_1 \to \mu^+\mu^- Z_2}$.

$$
\begin{aligned}
\mathcal{L} &= \frac{N_{\text{beam}}}{\sigma_{z-beam}/c}\, n_{\text{target}}\, T_{\text{target}} \\
\mathcal{R}_{\gamma Z_1 \to \mu^+\mu^- Z_2} \text{ (in 50fs)} &= \frac{1\text{nC}}{e}\, 5.9 \times 10^{28} m^{-3}\, 1cm\, 0.5 \text{ milli-barn} \\
\mathcal{R}_{\gamma Z_1 \to \mu^+\mu^- Z_2} \text{ (in 50fs)} &\simeq 10^5 \text{ pairs (1nC, 50fs, } \sigma_r \sim 20\mu m)
\end{aligned}
\tag{5}
$$

where,

N_{beam}, σ_{z-beam} are the number of particles and the bunch length of the beam, respectively

n_{target}, T_{target} are the number density and the thickness of the target

The estimated number of muon pairs per 10GeV electron is thus between $10^{-4} - 10^{-5}/e$. For nominal FACET-II parameters[50] it is estimated that 10^5 pairs can be produced when electron beam with $N_{\text{beam}} = \frac{1\text{nC}}{e} \simeq 6.24 \times 10^9$ in 50fs bunch length is incident on Gold target (Au) with number density $n_{\text{target}} = 5.9 \times 10^{28} m^{-3}$ and target thickness, $T_{\text{target}} = 10^{-2} m$. The cross-section of BH muon pair production is 0.5 milli-barn as estimated in eq.4.

The energy spectrum of the muon pairs photo-produced by (R.2) is exponential and it peaks slightly above $2m_\mu c^2$. This implies that a large number of muons have

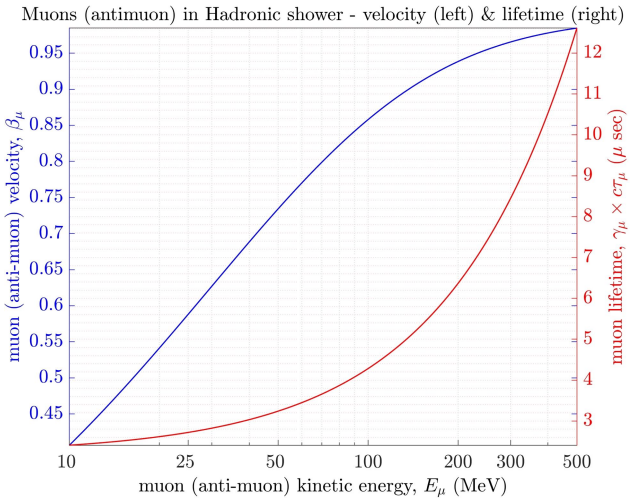

Fig. 2. Photo-produced Hadronic shower with an exponential velocity distribution has the shown muon velocity (β_μ) and corresponding lifetime ($\gamma_\mu \tau_\mu$) over a range of muon kinetic energy.

a low velocity. The angle of propagation of the muons is directly proportional to their relativistic momentum or the Lorentz factor.

In Fig.2, the properties of muons and antimuons contained a photo-produced hadronic shower are captured. The left-hand axis shows the muon (and antimuon) velocity while the right-hand axis their corresponding lifetime.

The energy spectrum and transverse phase-space of the particles in a hadronic shower are therefore unconstrained. In the laser muon acceleration scheme introduced here, the photo-produced hadronic shower which primarily comprises of muon pairs is coupled into a laser-driven slowly propagating acceleration structure in the plasma. This slowly propagating laser acceleration structure traps the charged particles and accelerates them.

From a comparison of Fig.2 on hadronic shower muon properties and Fig.1 on laser group velocity it is apparent that to trap muons with greater than 10MeV kinetic energy and velocities around 0.5c, it is necessary to use plasma densities as high $10^{20} cm^{-3}$.

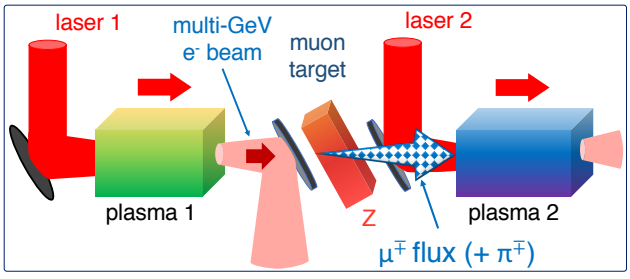

Fig. 3. Schematic of laser-plasma post-processing of photo-produced (photo-meson and BH muon pair-production) $\pi^{\pm}$-$\mu^{\pm}$ Hadronic shower driven by $e^{\pm}$ beam in a target.

5.2. *Scheme II: Laser-driven plasma based post-processing of proton beam driven hadronic shower*

When proton beam is shot onto a target, direct interaction of protons with atomic nuclei dominates the interaction. The resulting proton-nucleon reaction result in the production of pions mediated by the strong force. These reactions occur between the high-energy protons in the beam and the nucleons that constitute the atomic nuclei:

(R.3) protons, $p + p \rightarrow \pi^+ + p + p$

(R.4) neutrons, $p + n \rightarrow \pi^- + p + p$

Thus, the hadronic shower produced is primarily a pion shower. The threshold proton beam energy required can be estimated from momentum four-vector of the interaction:

$$E_p^{\rm th}\Big|_{\pi^\pm} = \left[\frac{1}{2}\left(2 + \frac{m_{\pi^\pm}}{m_p}\right)^2 - 2\right] m_p c^2 \simeq 0.31\ m_p c^2 \sim 290\ \text{MeV} \tag{6}$$

The cross-section of proton-nucleon reactions which is dictated by strong interactions is,

$$\begin{aligned} \sigma_{pp}(E_p) &\simeq 40 \times 10^{-27}\ cm^{-2} = 40\ mb, \quad (1\text{barn} = 10^{-24} cm^{-2}) \\ \sigma_{pZ}(Z,A) &\simeq \sigma_{pp} \times A^{0.7} \quad [\sigma_{pZ}(A > 100) \simeq 1\ \text{barn}] \end{aligned} \tag{7}$$

The event-rate of pion production is calculated for a hypothetical ultra-short (< 1 ps) 500MeV proton bunch with 1nC charge ($N_{beam} = 6.24 \times 10^9$ protons) incident on a 1cm thick Tungsten ($\text{A}_\text{W}(\text{Z} = 74) \simeq 184$) target of number density $n_{\rm target} = 6.3 \times 10^{22} cm^{-3}$ using below,

$$\begin{aligned} \mathcal{L} &= \frac{N_{\rm beam}}{\sigma_{z-beam}/c}\ n_{\rm target}\ T_{\rm target} \\ \mathcal{R}_{pZ\rightarrow\pi^\pm pZ} &= \frac{dN_{\mu^\pm}}{dt} = \mathcal{L} \times \sigma_{pZ} \\ &= \frac{1\text{nC}}{e}\ 6.3 \times 10^{28} m^{-3}\ 1cm\ 1.54\ \text{barn} \quad = 6.1 \times 10^8\ \pi^\pm \end{aligned} \tag{8}$$

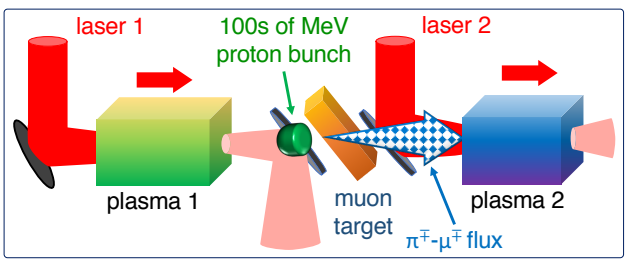

Fig. 4. Schematic of laser-plasma post-processing of proton-neutron reaction based $\pi^\pm$-$\mu^\pm$ hadronic shower driven by proton beam in a target.

This pion production process is thus quite efficient relative to the photo-production process as it produces 0.1 pion per proton. It is also however well known that 0.5GeV proton beams that can be focussed down to micron-scale spot-size are not available in ultra-short pico-second scale bunches with 1nC scale charge. Therefore, this scheme relies on a possible yet currently non-existent proton beam.

The energy spectrum and transverse phase-space of the shower pions is not usable in any real applications. This demands capture and storage of pions in a ring before they predominantly decay to muons.

In this laser muon acceleration scheme, the charged pions in the proton beam driven hadronic shower are coupled into a slowly propagating acceleration structure in the plasma. This slowly propagating laser-driven plasma acceleration structure traps the charged pions (thus, does not trap π^0) and accelerates them to high energies. Relativistic pions decay in a small forward angle and thus acceleration of pions is essential to increase the capture efficiency of muons produced from pion decay. However, the meters long pion confinement channel needed after the laser acceleration stage does not allow for a compact design.

5.3. *Scheme III: Laser-plasma positron electron mini-collider storage ring*

Standalone laser-plasma electron accelerators have been shown to produce multi-GeV beams which undergo bremsstrahlung in a metal target which results in BH pair production of positrons and electrons. The resulting particle shower is post-processed using a laser-driven plasma stage to trap and accelerate a positron and electron dual bunch beam. The proof-of-principle of a positron laser-plasma accelerator has been demonstrated[5] and is currently under active investigation[6].

These beams are stored in a mini-Collider ring where at the interaction or collision point muon pairs are produced close to their resonance from electron positron annihilation mediated by a virtual photon of the collision point energy. Energy asymmetry between the positron and electron beams is preferable as the produced muon pairs then have an initial kinetic energy and can thus be injected into a subsequent acceleration stage.

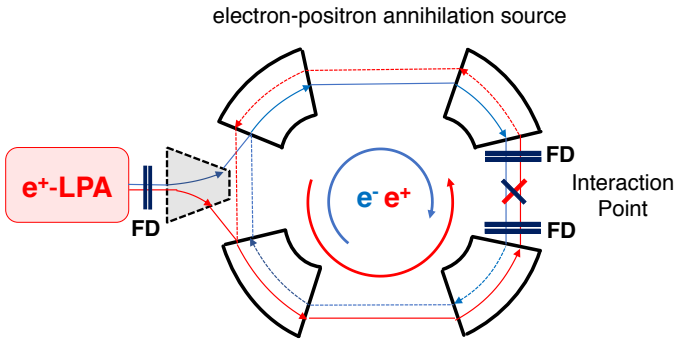

Fig. 5. Schematic of a muon source using mini Collider based upon laser-plasma positron electron storage ring .

Positron-electron annihilation allows access to the frontiers of center-of-mass energy and have thus been tools for discovering new physics. Advances in accelerator physics strive to make these tools compact and affordable. However, in this scheme a mini-Collider with a tunable energy symmetry between the colliding electron and positron beam energy enables the production of tunable energy muon beams.

During the collision of unpolarized spin electron and positron beams, the annihilation differential cross-section of muon pair production (which exhibits the typical QED $1/s$ dependence of the cross-section) is,

$$\begin{aligned}\frac{d\sigma_{e^\pm\to\mu^\pm}}{d\Omega} &\simeq \frac{e^4}{64\pi^2}\frac{\hbar^2c^2}{s}\,\frac{\sqrt{s-4m_\mu^2}}{\sqrt{s-4m_e^2}}\left(1+4\frac{(m_e^2+m_\mu^2)}{s}+\left(1-\frac{4m_e^2}{s}\right)\left(1-\frac{4m_\mu^2}{s}\right)\cos^2\theta\right)\\ \frac{d\sigma_{e^\pm\to\mu^\pm}}{d\Omega} &\simeq \frac{e^4}{64\pi^2}\frac{\hbar^2c^2}{s}\left(1+\cos^2\theta\right)\quad (\text{under, } \sqrt{s}\gg m_\mu > m_e)\end{aligned} \tag{9}$$

and the integrated cross-section of electron-positron annihilation during collision to muon-antimuon pair is,

$$\sigma_{e^\pm\to\mu^\pm} = \int\left(\frac{d\sigma_{e^\pm\to\mu^\pm}}{d\Omega}\right)\,d\Omega = \frac{4\pi}{3}\,\alpha^2\,\frac{\hbar^2c^2}{s} = \frac{87\text{ nbarns}}{\text{s (in GeV}^2)} \tag{10}$$

where,

$\sigma_{e^\pm\to\mu^\pm}$ is the cross-section of the reaction electron-positron collision to muon-antimuon pair production
Ω is the solid angle in the real space
m_e, m_μ are electron and muon mass respectively
s is the norm of the summed momentum four-vectors of electron ($\mathbf{p}$) and positron ($\tilde{\mathbf{p}}$) beam at the point of collision ($\|\mathbf{p}+\tilde{\mathbf{p}}\|^2$),
it is also the norm of the summed muon (k) and anti-muon ($\tilde{k}$) momentum four-vectors at the point of collision ($\|\mathbf{k}+\tilde{\mathbf{k}}\|^2$)
θ is the angle between $\mathbf{p}$ and $\mathbf{k}$
α is the fine structure constant

The event rate ($\mathcal{R}_{e^\pm\to\mu^\pm} \equiv dN_{\mu^\pm}dt^{-1}$) muon-antimuon pair-production in positron-electron beam (assumed to have a Gaussian spatio-temporal profile) collision which depends on the luminosity ($\mathcal{L}$, $\text{cm}^{-2}\text{s}^{-1}$) parameter is therefore, and the integrated cross-section of electron-positron annihilation during collision to muon-antimuon pair is,

$$\begin{aligned}\mathcal{L} &= \frac{N^{e^+}N^{e^-}}{4\pi\;\sigma_r^{e^+}\sigma_r^{e^-}}\;\hat{S}\;f_{rep}\quad (\text{equal bunchlengths}, \sigma_{\text{s}}^{\text{e}^+}\sigma_{\text{s}}^{\text{e}^-})\\ \mathcal{R}_{e^\pm\to\mu^\pm}(\text{per collision}) &\equiv \frac{dN_{\mu^\pm}}{dt} = \mathcal{L}\times\sigma_{e^\pm\to\mu^\pm} = \frac{1}{s}\;\frac{\alpha^2}{3}\;\frac{N^{e^+}N^{e^-}}{\sigma_r^{e^+}\sigma_r^{e^-}}\;\hat{S}\\ &= \frac{7}{\text{s (in GeV}^2)}\;\frac{N^{e^+}N^{e^-}}{\sigma_r^{e^+}\sigma_r^{e^-}}\;\hat{S}\end{aligned} \tag{11}$$

where,

$\sigma_r^{e^+}$, $\sigma_r^{e^-}$ is the radial waist-size of radially symmetric positron and electron bunches of spatio-temporal Gaussian profile, respectively.

N^{e^+}, N^{e^-} is the number of particles in Gaussian positron and electron bunches, respectively.

$\hat{S}$ is the Luminosity reduction factor due to several practical considerations such as crossing angles, Non-Gaussian profiles, Hourglass effect due to tight focussing, collision offsets etc.

f_{rep} is the number of collision per second

For this scheme, we assume that laser-plasma accelerator produced positron and electron bunches of 200 pC ($N^{e^+} \sim N^{e^-} \simeq 1.25 \times 10^9$ particles per bunch) each are coupled to a storage ring and are made to collide at a collision point with tightly focused beam waist-size of $\sigma_r^{e^+} \simeq \sigma_r^{e^-} \simeq 10^{-10}m = 0.1$ nm (difficult, if not impossible). Assuming that the electron beam energy is $E_{e^-} = 150MeV$ and that of the positron beam is $E_{e^+} = 100MeV$ then the number of muon pairs produced is only about $\simeq 1500$ with an initial kinetic energy of few 10s of MeV.

So, while the mini collider-based scheme produces beams of small spot-size, bunch length and transverse emittance, it is quite ineffective at scaling the number of muons at each collision event.

6. Particle In Cell Simulation of Scheme 1: Controlled interaction of μ^+-μ^- pair-plasma with laser-driven plasma

Multi-dimensional PIC simulations are used to validate the laser muon acceleration schemes outlined above, especially with relevance to the Scheme I (section 5.1). The PIC simulation reported below use the open-source EPOCH code[51]. In this section, $2\frac{1}{2}$D simulations adjusted to match 3D simulations are presented for preliminary evaluation of trapping and acceleration of muons. In these simulations, a 2D cartesian grid which resolves $\lambda_0 = 0.8\mu$m with 20 cells in the longitudinal and 15 cells in the transverse direction tracks a linearly-polarized laser pulse at its group velocity.

The photo-produced hadronic particle shower driven by multi GeV electron beam shows a peak in its energy spectrum around muon energy of 200MeV[48]. In the simulation results presented in this section, the hadronic shower (made only of μ^- particles) is initialized with transverse size of $\sigma_r = 20\mu m$ and the shower longitudinally spans the entire simulations box. Each particle species is initialized with 4 particles per cell. Absorbing boundary conditions are used for both fields and particles. A 1J laser with a Gaussian envelope of 30fs pulse length is focussed to a spot-size of $w_0 = 5\mu m$ at the plasma and propagates in 50μm of free-space before it impinges on a fixed-ion plasma.

The preliminary $2\frac{1}{2}$D PIC simulations carried out as described above provide good understanding of the process of trapping and acceleration of muons contained within the hadronic shower or muon-antimuon pair-plasma. Below we present a few

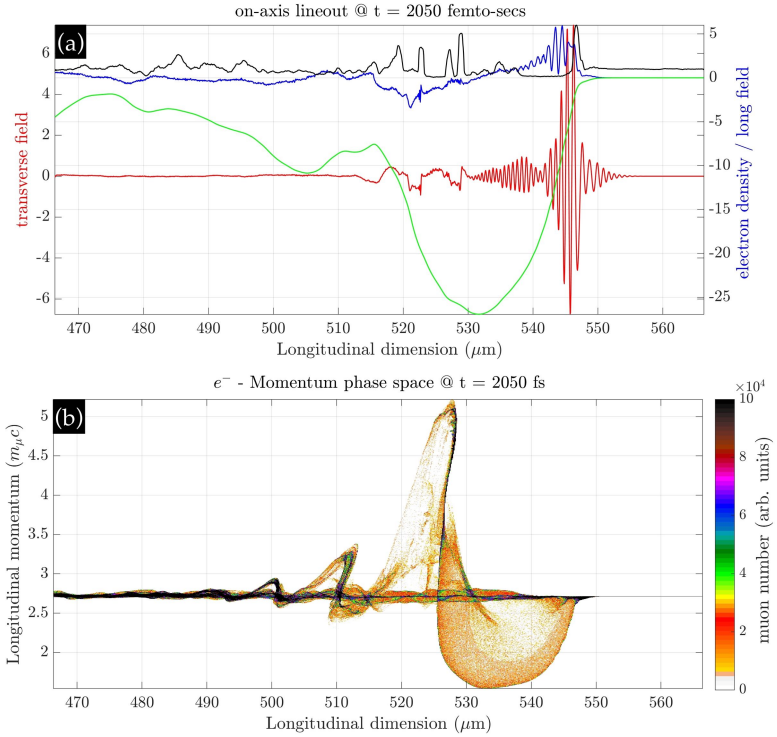

Fig. 6. On-axis lineout of laser-plasma interaction parameters (in a) and muon (μ^-) momentum phase space (in b), with muon longitudinal momentum shown along the longitudinal dimension at around 2ps and about 0.6mm of plasma length. The initialized 200MeV muons get trapped and accelerated in laser plasma acceleration structures driven using a 1J, 30fs laser focussed to a focal spot-size of $w_0 = 5\mu m$ interacting with a laser-ionized $n_0 = 2 \times 10^{19}\text{cm}^{-3}$ plasma.

$2\frac{1}{2}$D PIC simulation snapshots (Fig.6 to 10) to establish the viability of laser muon acceleration for a pre-ionized $n_0 = 2 \times 10^{19}\text{cm}^{-3}$ plasma.

The $2\frac{1}{2}$D PIC simulation snapshots presented as evidence of laser muon acceleration are as follows:

(1) Fig.6(a) shows the on-axis lineout of various laser-plasma parameters (laser transverse field is normalized to $m_e c\omega_0 e^{-1}$, longitudinal plasma field is normalized to $m_e c\omega_{pe} e^{-1}$, plasma electron density, n_0(initial), plasma potential is normalized to $m_e c^2 e^{-1}$). Fig.6(b) shows corresponding muon longitudinal momentum phase-space with longitudinal muon momentum along the y-axis and longitudinal dimension along the x-axis. From this phase-space, it is clear that the muons gain around 200MeV over 0.6mm.

(2) Fig.7 shows the 2D real-space simulation snapshot of: plasma electron density of the acceleration structure (in a), plasma longitudinal field (in b) and laser transverse field (in c) corresponding to the time snapshot in Fig.6.

(3) Fig.8 shows the 2D real-space simulation snapshot of trapped and accelerated muon bunch density.

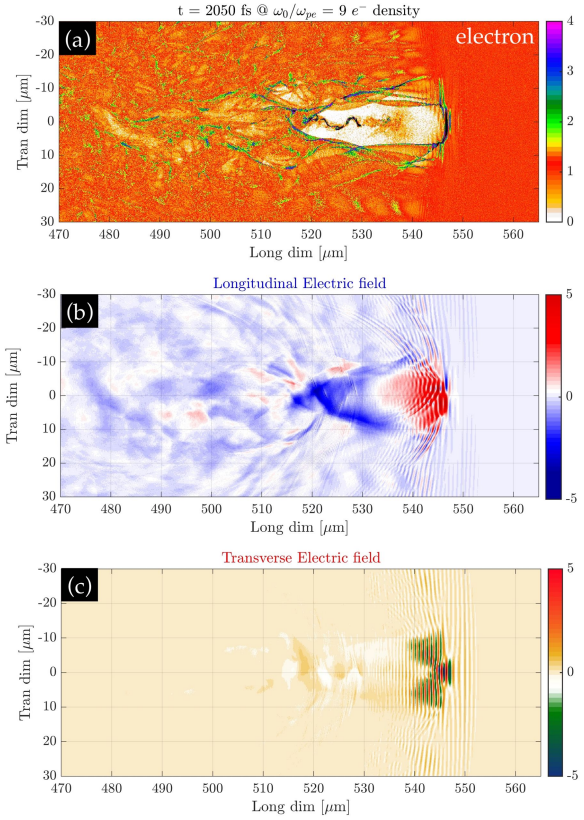

Fig. 7. Laser-plasma interaction characteristics (normalized) of laser muon accelerator corresponding to the on-axis lineout in Fig.6(a) at around 2ps in a $n_0 = 2 \times 10^{19}\text{cm}^{-3}$ plasma: (a) plasma electron density of the acceleration structure, (b) longitudinal electric field associated with the plasma acceleration structure, (c) the transverse field of the evolving laser pulse.

(4) Fig.9 shows the muon momentum phase-space of longitudinal momentum along the y-axis against transverse real-space along the x-axis. From this snapshot it can be inferred that muons have small amplitude transverse oscillations as they gain energy. Additionally, the accelerated beam transverse spot-size can be inferred to be $< 10\mu$m.

(5) Fig.10 shows the muon momentum phase-space of longitudinal momentum along the y-axis against transverse momentum along the x-axis. This snapshot further reinforces the transverse dynamics of muons as they gain energy. Moreover, it shows that < 10mrad opening angles are likely from a laser muon accelerator.

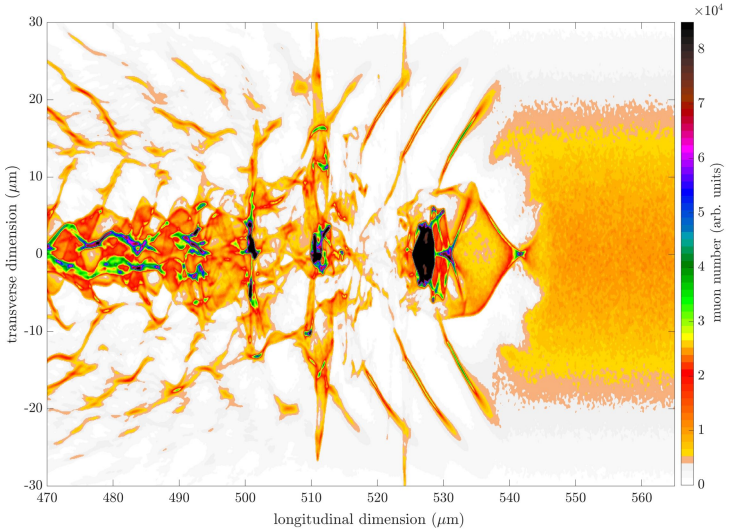

Fig. 8. Trapped and accelerated muon (μ^-) bunch in real space with micron-scale transverse and longitudinal dimensions at around 2ps of laser-plasma interaction corresponding with the laser muon acceleration snapshot presented in Fig. 7 in a $n_0 = 2 \times 10^{19}\text{cm}^{-3}$ plasma.

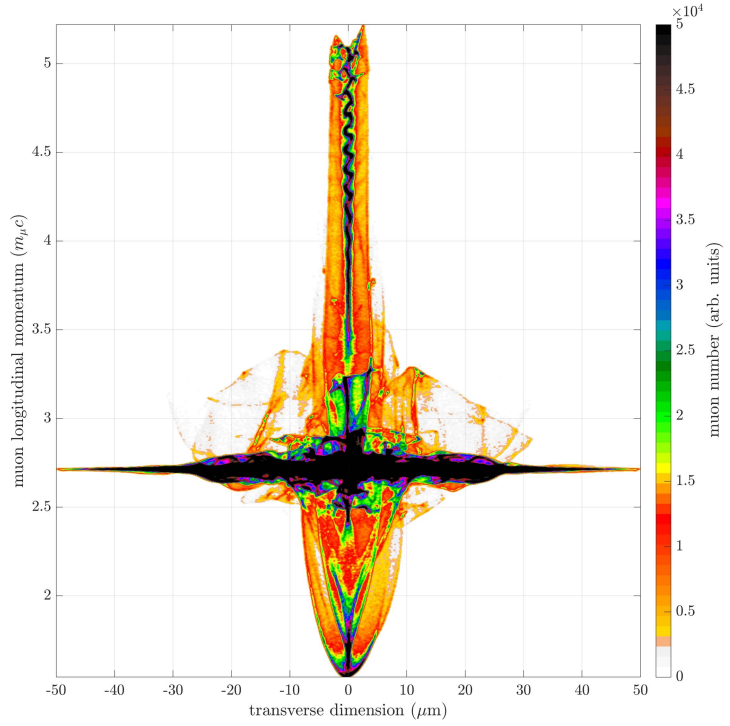

Fig. 9. Muon (μ^-) momentum phase space, with muon longitudinal momentum along the y-axis shown against the transverse real-space dimension along the x-axis at around 2ps and about 0.6mm of laser propagation in plasma in correspondence with the snapshots presented in above figures.

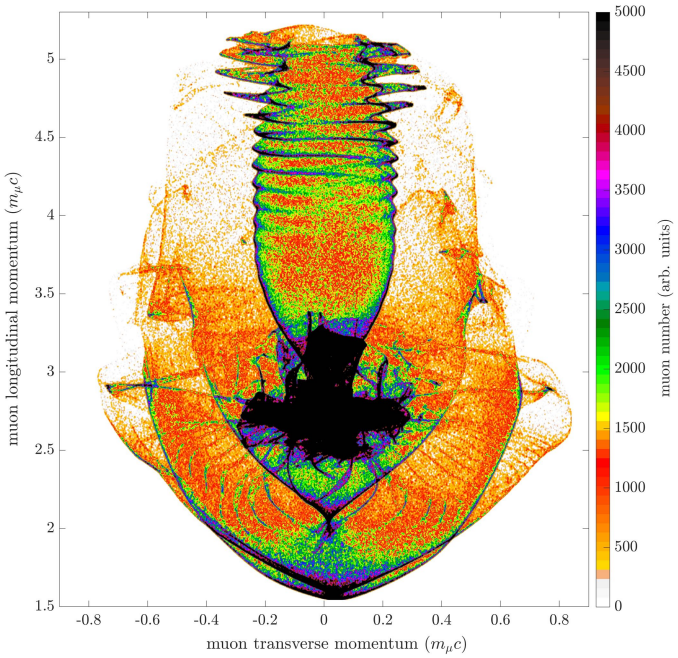

Fig. 10. Muon (μ^-) momentum phase space, with muon longitudinal momentum along the y-axis shown against the transverse momentum along the x-axis at around 2ps and about 0.6mm of laser propagation in plasma in correspondence with the snapshots presented in above figures.

From analysis of the simulation snapshots it can be inferred that acceleration of ultrashort, micron-scale muon beams is viable using laser muon accelerator even with a few tens of TW peak power CPA laser.

7. Conditioning-Stage Using a Plasma Lens: Charge Dependent Focusing of Oppositely Charged Particles

The proposed conditioning step involves the use of a discharge plasma lens to segregate oppositely charged species of a particle-shower or an oppositely charged dual bunch configuration by selectively focusing one charge sign of the particles.

Cascade shower (electromagnetic or hadronic) that contains both the oppositely charged particle species such as electron-positron ($e^{\pm}$) pair or muon-anti muon ($\mu^{\pm}$) pair, is produced for instance using an electron and/or positron beam or a proton beam. These beams are themselves possibly obtained using a laser-plasma accelerator. In the plasma lens based conditioning stage, the oppositely charged species of the cascade shower are selectively segregated due to only one of the charge sign being focused in the device while the other is de-focused.

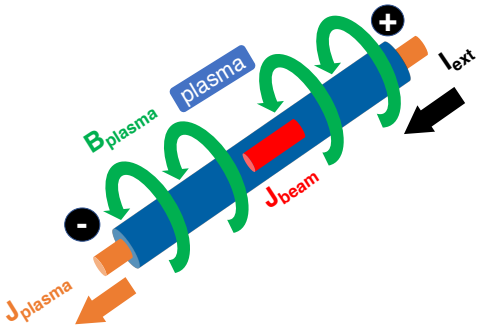

$$B_\phi(r < R_{\rm lens}) = C_1\ J_0\ \frac{r^{\alpha+1}}{R^\beta}$$

$$\frac{\partial v_r}{\partial z} + k_{\rm lens}^2\ r = \frac{\partial^2 r}{\partial z^2} + k_{\rm lens}^2\ r = 0$$

$$k_{\rm lens}^2 = \pm e\ C_2\ J_0\ \frac{r^\alpha}{R^\beta}\ \frac{1}{p_z}$$

Fig. 11. Schematic of the conditioning stage where a discharge plasma lens[52] is used to segregate species of opposite charge sign by phasing the discharge current direction (if RF voltage is applied).

The plasma lens is based upon a discharge plasma where a high RF terminal voltage is applied to sustain the discharge. By appropriately phasing the entrance phase of the cascade shower and the RF voltage phase it is possible to choose the charge sign to be focused.

With the choice of amplitude and polarity of the externally injected current, discharge plasma dimensions, gas pressure and gas type it is possible to control the acceptance and focusing properties of the cascade shower processing device.

In the 1965[52] BNL work on using plasma discharges as active plasma lens it was also found that the focusing strength of an active plasma lens was directly proportional to the radial distance from the axis (particles away from the axis experience higher focusing force) and inversely proportional to the momentum of the cascade shower particle (lower energy particles experience higher focusing force).

These focusing characteristics of the discharge plasma lens can be understood if the problem is considered in a cylindrical coordinate system (r, z, ϕ) as depicted in Fig.11. The azimuthal field in plasma ($B_{\rm plasma} = B_\phi$) is excited due to the plasma current ($J_{\rm plasma} = J_0$) which is driven by externally injected current, $I_{\rm ext}$ along the z direction. This azimuthal magnetic field due to the plasma current exerts a force on longitudinally (along z) propagating charged particle beam. The Lorentz force on the charged beam particle injected along z interacting with a magnetic field oriented along is in the radial, r direction. The equation of radial motion of each charged particle in the beam is governed by the lens equation above.

Cascade showers comprising of oppositely charged particle species generated by the decay of high-energy gamma-ray photons in a metallic target have energy spectra which has a concentration of particles at non-relativistic energies. However, due to the randomized decay of high-energy gamma-rays, the divergence angle of

the particle shower particles can be large. A plasma lens that is located right next to a metallic converter target can also capture the divergent charged particles of the cascade shower.

Depending upon the direction of the discharge plasma current one of the charged particle species is focused and the other is defocused. This leads to the segregation of the oppositely charged particle species of the cascade shower. Therefore, at the output of the assembly of particle-shower target and plasma lens one of the charged particle species is detectable whereas the species with the opposite sign of charge is excessively defocussed and thus diluted.

8. Discussion and Future Work

In this paper, experimentally viable and affordable laser muon sources have been introduced in consideration of the numerous possibilities offered for a wide-range of applications. This paper proposes and estimates the experimental viability of compact and tunable schemes of laser muon acceleration in gas plasmas using an innovative technique of post-processing of muon-antimuon cascade hadronic showers or pair plasmas through their controlled interaction with laser-driven plasmas.

The laser muon acceleration schemes introduced and investigated here are designed in consideration of being well within the reach of experimental verification using existing experimental facilities as reflected in the choice of experimental setup and laser, plasma and beam parameters. Although the first-stage of the muon acceleration schemes presented here rely on laser accelerated particles such as multi GeV electrons, for proof-of-principle experiments may be based on more controlled and reliable 10 GeV scale electron beams from rf accelerators, in the short-term.

In the short term, the scheme I (section 5.1) which uses direct photo-production of muon pairs, although being limited in overall conversion efficiency, is found to be most suitable for the development of an experimental prototype of a laser muon accelerator that produces ultrashort and micron-scale muon beam. A few facilities, like BELLA at Berkeley and FACET-II at Stanford, that offer collocated CPA laser and micron-scale e^- and/or e^+ beams of many 10s to 100s of pC charge at 10 GeV scale beam energy, can be utilized for this prototyping effort.

Preliminary PIC simulations presented in section 6 demonstrate the potential to trap and accelerate muons in gas plasmas. In these simulations, we observe several 100MeV gain in muon energy in less than a millimeter. Further modeling using analysis, particle-tracking and particle-in-cell simulations will be carried out to accurately estimate the properties of the accelerated muon beams within the reach of an experimentally viable laser muon accelerator prototype. In future work, we thus propose to extend the preliminary Particle-In-Cell based modeling of laser muon acceleration schemes reported here along with substantially more detailed modeling of muon photo-production using micron-scale electron or positron beams.

We will model the possibilities of tunable and spectrally controlled acceleration of muon and antimuon beams, dual bunch muon-antimuon beams, spatio-temporally

overlapped electron and muon bunch beams, increasing the total trapped muon beam charge, segregation of oppositely charged muons prior to the acceleration stage etc. Moreover, our experimental prototyping effort will work hand-in-hand with theoretical modeling to better understand the expected muon cascade shower or pair-plasma properties and its interaction with laser-driven plasmas.

Compact and tunable production and acceleration of unprecedented ultra-short (femtosecond to attosecond) micro-scale spot muon beams is essential for an advanced acceleration program using muons and suited for acceleration mechanisms with inherently micron to nanometer spatial scale. Moreover ultrashort, micron-scale muon beams can be injected into crystal wakefield accelerators such as attosecond x-ray pulse driven[11–13] or sub-micron particle beam driven solid-state tube accelerators[14,15] in order to minimize the synchrotron radiation losses ($\propto m_\mu^{-4}$) as well as the radiative losses ($\propto m_\mu^{-2}$) in comparison with electrons and positrons. The significance of a compact tunable high-energy muon source also importantly lies in its multitude of technological, security and medical applications.

9. Acknowledgments

A. A. S. was supported by the College of Engineering and Applied Science, University of Colorado, Denver. V. D. S. was supported by Fermi National Accelerator Laboratory, which is operated by the Fermi Research Alliance, LLC under Contract No. DE-AC02-07CH11359 with the United States Department of Energy. This work utilized the RMACC Summit supercomputer through the XSEDE program, which is supported by the National Science Foundation (awards ACI-1532235 and ACI-1532236), the University of Colorado Boulder, and Colorado State University. The Summit supercomputer is a joint effort of the University of Colorado Boulder and Colorado State University[53].

References

1. Tajima, T., Dawson, J. M., *Laser Electron Accelerator*, Phys. Rev. Lett. **43**, 267 (1979)
2. Strickland, D., Mourou, G., *Compression of amplified chirped optical pulses*, Optics Communications **56**, Issue 3, p. 219 (1985)
3. Leemans, W. P., Gonsalves, A. J., Mao, H.-S., Nakamura, K., Benedetti, C., et. al., *Multi-GeV Electron Beams from Capillary-Discharge-Guided Subpetawatt Laser Pulses in the Self-Trapping Regime*, Phys. Rev. Lett. **113**, 245002 (2014) Wang, X., Zgadzaj, R., Fazel, N., Li, Z., et. al., *Quasi-monoenergetic laser-plasma acceleration of electrons to 2 GeV*, Nature Communications **4**, 1988 (2013)
4. Kim, H. T., Pae, K. H., Cha, H. J., Kim, I. J., et. al., *Enhancement of Electron Energy to the Multi-GeV Regime by a Dual-Stage Laser-Wakefield Accelerator Pumped by Petawatt Laser Pulses* Phys. Rev. Lett. **111**, 165002 (2013); Steinke, S., van Tilborg, J., Benedetti, C., Geddes, C. G. R., et. al., *Multistage coupling of independent laser-plasma accelerators*, Nature **530**, pp.190-193 (2016);
5. Sahai, A. A., *Quasimonoenergetic laser plasma positron accelerator using particle-shower plasma-wave interactions*, Phys. Rev. Accel. Beams **21**, 081301 (2018)
6. Sahai, A. A., Thomas, A. G., Cary, J. R., Golkowski, M., Harid, V., Geddes, C. G.,

Tajima, T., *Laser Positron Accelerator: Proof-of-Principle experimental effort and Novel Applications*, LaserNetUS Expt. proposal

7. Xie, M., Tajima, T., Yokoya, K., Chattopadhyay, S., *Studies of laser-driven 5 TeV colliders in strong quantum e^+e^- beamstrahlung regime*, AIP Conference Proceedings 398, 233 (1997); Leemans, W., Esarey, E., *Laser-driven plasma-wave electron accelerators*, Physics Today **62**, 3, pp.44-49 (2009)
8. Uesaka, M., Koyama, K., *Advanced accelerators for medical applications*, Reviews of Accelerator Science and Technology, **9**, pp. 235-260 (2016)
9. Albert, F., Thomas, A. G.R., *Applications of laser wakefield accelerator-based light sources*, Plasma Physics and Controlled Fusion **58**, 10, p.103001 (2016)
10. Yukawa, H., *On the Interaction of Elementary Particles. I*, Proc. of the Physico-Mathematical Society of Japan **17** pp.48-57 (1935); Neddermeyer, S. H., Anderson, C. D., *Note on the Nature of Cosmic-Ray Particles*, Phys. Rev. **51**, pp.884-886 (1937)
11. Tajima, T., Cavenago, M., *Crystal x-ray accelerator*, Phys. Rev. Lett. **59**, 1440 (1987), doi:10.1103/PhysRevLett.59.1440
12. Hakimi, S., Nguyen, T., Farinella, D., Lau, C. K., Wang, H.-Y., Taborek, P., Dollar, F., Tajima, T., *Wakefield in solid state plasma with the ionic lattice force*, Physics of Plasmas **25**, p. 023112 (2018)
13. Hakimi, S., Zhang, X. Lau, C., Taborek, P., Dollar, F., Tajima, T., *X-ray Laser Wakefield Acceleration in a Nanotube*, Proceedings of the **XTALS 2019** workshop on Acceleration in Crystals and Nanostructures.
14. Chen, P., Noble, R. J., *A Solid State Accelerator*, American Inst. Physics Conference Proceedings **156**, 222 (1987); Chen, P., Noble, R. J., *Crystal Channel Collider: Ultra-High Energy and Luminosity in the next century*, AIP Conference Proceedings **398**, 273 (1997) [SLAC-PUB-7402 (1998)]
15. Sahai, A. A., Tajima, T., Shiltsev, V. D., Taborek, P., *Solid-state Tube Wakefield Accelerator using surface waves in crystals*, Proceedings of the **XTALS 2019** workshop on Acceleration in Crystals and Nanostructures.
16. Shiltsev, V. D., *High-energy particle colliders: past 20 years, next 20 years, and beyond*, Physics-Uspekhi, **55**, 10, p.265 (2012)
17. Nagamine, K., Cambridge University Press (2003), ISBN:9780511470776
18. Palmer, R. B., Sessler, A., Skrinsky, A., Tollestrup, A., Blatz, A. J., et. al, AIP Conference Proceedings **372**, 3 (1996) [arXiv:acc-phys/9602001]; Muon Collider Collaboration, *Status of muon collider research and development and future plans*, Phys. Rev. ST Accel. Beams, **2**, 081001 (1999);
19. Williams, E. J., Roberts, G. E., *Evidence for Transformation of Mesotrons into Electrons*, Nature 145, p.102 (1940)
20. Kosharev, D. G., *Proposal for a decay ring to produce intense secondary particle beams at the SPS*, CERN Report No. CERN/ ISR-DI/74-62 (1974); Geer, S., *Neutrino beams from muon storage rings: Characteristics and physics potential*, Phys. Rev. D **57**, 6989 (1998);
21. Moretti, A., Qian, Z., Norem, J., Torun, Y., Li, D., Zisman, M., *Effects of high solenoidal magnetic fields on rf accelerating cavities*, Phys. Rev. ST Accel. Beams **8**, 072001 (2005); Palmer, R. B., Fernow, R. C., Gallardo, J. C., Stratakis, D., Li, D., *rf breakdown with external magnetic fields in 201 and 805 MHz cavities*, Phys. Rev. ST Accel. Beams **12**, 031002 (2009)
22. Wideroe, R., *Uber ein neues Prinzip zur Herstellung hoher Spannungen*, Archiv fur Elektrotechnik **21**, iss. 4, p.387 (1928)
23. Borozdin, K. N., Hogan, G. E., Morris, C., Priedhorsky, W. C., Saunders, A., Schultz, L. J., Teasdale, M. E., *Surveillance: Radiographic imaging with cosmic-ray muons*,

Nature **422**, p.277 (2003)

24. Morishima, K., Kuno, M., Nishio, Kitagawa, A. N., Manabe, Y., et. al., *Discovery of a big void in Khufuś Pyramid by observation of cosmic-ray muons*, Nature **552**, pp.386-390 (2017); Alvarez, L. W., Anderson, J. A., El Bedwei, F., Burkhard, J., Fakhry, A., et. al., *Search for hidden chambers in the pyramids*, Science **167**, iss.3919, pp.832-839 (1970)
25. Lesparre, N., Gibert, D., Marteau, J., Declais, Y., Carbone, D., Galichet, E., *Geophysical muon imaging: feasibility and limits* Geophysical Journal International **183**, iss. 3, pp.1348-1361 (2010); Jourde, K., Gibert, D., Marteau, J., de Bremond dArs, J., Komorowski, J-C., *Muon dynamic radiography of density changes induced by hydrothermal activity at the La Soufriere of Guadeloupe volcano*, Scientific Reports **6**, 33406 (2016)
26. Yamazaki, T., Nagamine, K., Nagamiya, S., Hashimoto, O., Sugimoto, K., et. al., *Negative Moun Spin Rotation*, Physica Scripta **11**, 133 (1975); Brewer, J. H., Fleming, D. G., Crowe, K. M., Johnson, R. F., Patterson, B. D., et. al., *mu+SR Spectroscopy: The Positive Muon as a Magnetic Probe in Solids*, Physica Scripta **11**, 144 (1975)
27. Barnabas, K. Venkateswaran, J. M. Stadlbauer, Z. Wu, D. C. Walker, *Contrasts between uracil and thymine in reaction with hydrogen isotopes in water*, J. Phys. Chem., **95** iss. 24, pp.10204-10207 (1991); Scheicher, R. H., Das, T. P., Torikai, E., Pratt, F. L., Nagamine, K., *First-principles study of muonium in A- and B-form DNA*, Physica B: Condensed Matter, **374-375**, pp.448-450 (2006)
28. Bossoni, L., Moursel, L. G., Bulk, M., Simon, B. G., Webb, A., et. al., *Human-brain ferritin studied by muon spin rotation: a pilot study*, Journal of Physics: Condensed Matter **29**, 415801 (2017); Nagamine, K., Shimomura, K., Imai, K., Schultz, J. S., *Probing magnetism in human blood by muon spin relaxation*, Physica B, **374-375** pp.444-447 (2006)
29. Fermi, E., Teller, E., *The Capture of Negative Mesotrons in Matter*, Phys. Rev. **72**, 399 (1947); Garwin, R. L., Lederman, L. M., Weinrich, M., *Observations of the Failure of Conservation of Parity and Charge Conjugation in Meson Decays: the Magnetic Moment of the Free Muon*, Phys. Rev. **105**, 1415 (1957)
30. Brodsky, S. J., Lebed, R. F., *Production of the Smallest QED Atom: True Muonium (μ^+-μ^-)*, Phys. Rev. Lett. **102**, 213401 (2009); Karshenboim, S. G., Jentschura, U. D., Ivanov, V. G., Soff, G., *Next-to-leading and higher order corrections to the decay rate of dimuonium*, Physics Letters B **424**, pp.397-404 (1998)
31. Jackson, J. D., *Catalysis of Nuclear Reactions between Hydrogen Isotopes by mu-minus Mesons*, Phys. Rev. **106**, 330 (1957); Alvarez, L. W., H. Brander, F. S. Crawford, Jr., J. A. Crawford, P. Falk-Variant, et. al., *Catalysis of Nuclear Reactions by mu-minus Mesons*, Phys. Rev. **105**, 1127 (1957)
32. Bose, D. M., Choudhuri, B., Sinha, M., *Cosmic-Ray Meson Spectra*, Phys. Rev. 65, 341 (1944); Lattes, C. M. G., Muirhead, H., Occhialini, G. P. S., Powell, C. F., *Processes involving charged mesons*, Nature **159**, pp.694-697 (1947);
33. Fermi, E., *High Energy Nuclear Events*, Progress of Theoretical Physics **5**, Iss. 4, pp.570-583, (1950); Kothari, D. S., *Fermi's Thermodynamic Theory of the Production of Pions*, Nature **173**, p.590 (1954)
34. Cywinski, R., Bungau, A. E., Poole, M. W., Smith, S., de Reotier, P. D., et. al., *Towards a dedicated high-intensity muon facility*, Physica B **404**, p.1024-27 (2009); Cartlidge, E., *Muon users consider going it alone*, Phys. World **19**, iss.12, p.13 (2006)
35. Balbekov, V. I., Mokhov, N. V., *Low budget muon source*, Proc. of Particle Acc. Conf.(PAC), Chicago, TPAH144, IL, USA (2001); Miyadera, H., Jason, A. J., Kurennoy, S. S., *Simulation of Large Acceptance Linac for Muon*, Proc. of PAC,

FR5REP071, Vancouver, BC, Canada (2009)
36. Sayed, H. K., Berg, J. S., *Optimized capture section for a muon accelerator front end*, Physical Review Special Topics-Accelerators and Beams, **17**, 7, p.070102 (2014)
37. McMillan, E. M., Peterson, J. M., White, R. S., *Production of Mesons by X-Rays*, Science **110**, iss. 2866, pp. 579-583 (1949); G. F. Chew, M. L. Goldberger, F. E. Low, Y. Nambu, *Relativistic Dispersion Relation Approach to Photomeson Production*, Phys. Rev. **106**, 1345 (1957)
38. Nagamine, K., Miyadera, H., Jason, A., Seki, R., *Compact muon source with electron accelerator for a mobile mSR facility*, Physica B **404**, pp.1020-1023 (2009)
39. Tsai, Y-S., *Pair production and bremsstrahlung of charged leptons*, Rev. Mod. Phys., **46**, 815 (1974)
40. Athar, H., Lin, G. L., Tseng, J. J., *Muon pair production by electron-photon scatterings*, Phys. Rev. D 64, 071302(R) (2001);
41. Serafini, L., Drebot, I., Bacci, A., Broggi, F., Curatolo, C., et. al., *A muon source based on plasma accelerators*, Nuclear Inst. and Methods in Physics Research, A (2018)
42. Breit, G., Wheeler, J. A., *Collision of Two Light Quanta*, Phys. Rev. **46**, 1087 (1934)
43. Muller, C., Deneke, C., Keitel, C. H., *Muon-Pair Creation by Two X-Ray Laser Photons in the Field of an Atomic Nucleus*, Phys. Rev. Lett. **101**, 060402 (2008)
44. Muller, C., Deneke, C., Ruf, M., Mocken, G. R., Hatsagortsyan, K. Z., Keitel, C. H., *Lepton Pair Production in High-Frequency Laser Fields*, Laser Physics **19**, (2009)
45. Antonelli, M., Boscolo, M., Di Nardo, R., Raimondi, P., *Novel proposal for a low emittance muon beam using positron beam on target*, Nuclear Instruments and Methods in Physics Research A **807** (2016); Burkhardt, H., Kelner, S. R., Kokoulin, R. P., *Production of muon pairs in annihilation of high-energy positrons with resting electrons*, CERN-AB-2003-002 (2003)
46. Ginzburg, I. F., Jentschura, U. D., Karshenboim, S. G., Krauss, F., Serbo, V. G., Soff, G., *Production of bound $\mu+\mu$- systems in relativistic heavy ion collisions* Phys. Rev. C **58**, 3565 (1998)
47. Kaplan, D. M., Hart, T., Allport, P., *Producing an Intense, Cool Muon Beam via e^+e^- Annihilation*, arXiv:0707.1546 (2006)
48. Titov, A. I., Kampfer, B., Takabe, H., *Dimuon production by laser-wakefield accelerated electrons.*, Phys. Rev. ST Acc. Beams **12**, 111301 (2009); Rao, B. S., Jeon, J. H., Kim, H. T., Nam, C. H., *Bright muon source driven by GeV electron beams from a compact laser wakefield accelerator*, arXiv:1804.03886
49. Barletta, W. A., Sessler, A. M., *Characteristics of a high energy $\mu^+\mu^-$ collider based on electro-production of muons*, Nuclear Instrumentation Meth. A 350, p.36 (1994)
50. Yakimenko, V., *Ultimate Beams at FACET-II*, **XTALS 2019**, Workshop on Beam Acceleration in Crystals and Nanostructures; Yakimenko, V., Meuren, S., Del Gaudio, F., Baumann, C., Fedotov, A., et. al., *Prospect of Studying Nonperturbative QED with Beam-Beam Collisions*, Phys. Rev. Lett. **122**, 190404 (2019)
51. Arber, T. D., Bennett, K., Brady, C. S., Lawrence-Douglas, A., Ramsay, M. G., et. al., *Contemporary particle-in-cell approach to laser-plasma modelling*, Plasma Phys. Control. Fusion, **57**, 113001 (2015)
52. Forsyth, E. B., Lederman, L. M., Sunderland, J., *The Brookhaven-Columbia Plasma Lens*, IEEE Transactions on Nuclear Science, **12**, p.872 (1965)
53. Towns, J., Cockerill, T., Dahan, M., Foster, I., Gaither, K., et. al., *XSEDE: Accelerating Scientific Discovery*, Computing in Science & Engineering **16**, pp. 62-74, (2014); Anderson, J., Burns, P. J., Milroy, D., Ruprecht, P., Hauser, T., Siegel, H. J., *Deploying RMACC Summit: An HPC Resource for the Rocky Mountain Region* Proceedings of **PEARC17**, New Orleans, LA, USA, July 09-13, (2017)